

DexMV: Imitation Learning for Dexterous Manipulation from Human Videos

Yuzhe Qin* Yueh-Hua Wu* Shaowei Liu* Hanwen Jiang* Ruihan Yang Yang Fu
Xiaolong Wang
UC San Diego

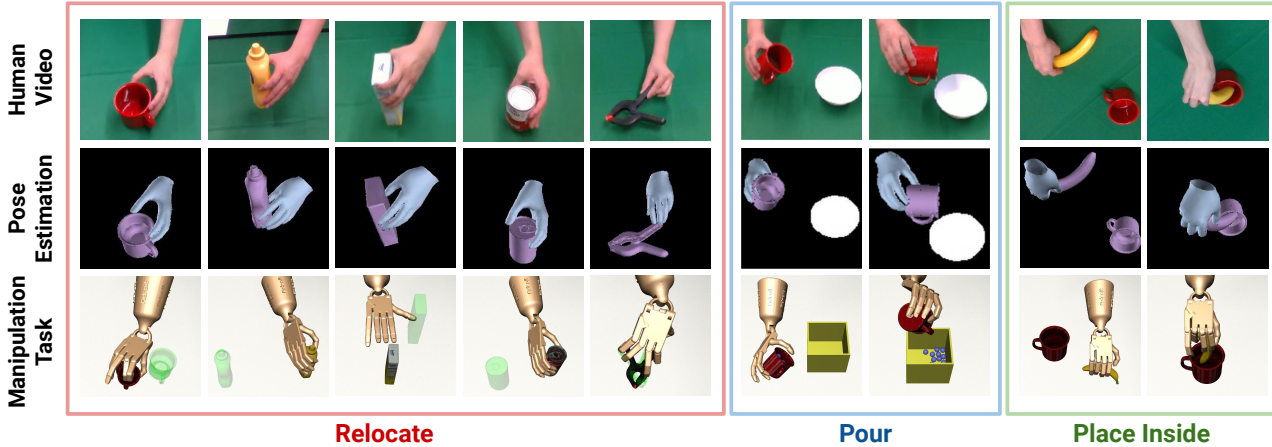


Figure 1: We propose to perform imitation learning for dexterous manipulation from human demonstration videos. We record human videos on manipulation tasks (1st row) and perform 3D hand-object pose estimations from the videos (2nd row) for constructing the demonstrations. We have a paired simulation system providing the same dexterous manipulation tasks for the multi-finger robot hand (3rd row), including *relocate*, *pour*, and *place inside*, which we can solve using imitation learning with the inferred demonstrations.

Abstract

While we have made significant progress on understanding hand-object interactions in computer vision, it is still very challenging for robots to perform complex dexterous manipulation. In this paper, we propose a new platform and pipeline, *DexMV (Dexterous Manipulation from Videos)*, for imitation learning to bridge the gap between computer vision and robot learning. We design a platform with: (i) a simulation system for complex dexterous manipulation tasks with a multi-finger robot hand and (ii) a computer vision system to record large-scale demonstrations of a human hand conducting the same tasks. In our new pipeline, we extract 3D hand and object poses from the videos, and convert them to robot demonstrations via motion retargeting. We then apply and compare multiple imitation learning algorithms with the demonstrations. We show that the demonstrations can indeed improve robot learning by a large margin and solve the complex tasks which reinforcement learning alone cannot solve. Project page with video: <https://yzqin.github.io/dexmv>.

1. Introduction

Dexterous manipulation of objects is the primary means for humans to interact with the physical world. Humans per-

form dexterous manipulation in everyday tasks with diverse objects. To understand these tasks, in computer vision, there is significant progress on 3D hand-object pose estimation [26, 85] and affordance reasoning [12, 17]. While computer vision techniques have greatly advanced, it is still very challenging to equip robots with human-like dexterity. Recently, there has been a lot of effort on using reinforcement learning (RL) for dexterous manipulation with an anthropomorphic robot hand [48, 47]. However, given the high Degree-of-Freedom joints and nonlinear tendon-based actuation of the multi-finger robot hand, it requires a *large amount* of training data with RL. Robot hands trained using only RL will also adopt *unnatural* behavior. Given these challenges, can we leverage humans' experience in the interaction with the physical world to guide robots, with the help of computer vision techniques?

One promising avenue is imitation learning from human demonstrations [59, 65]. Particularly, for dexterous manipulation, Rajeswaran *et al.* [59] introduces a simulation environment with four different manipulation tasks, and paired sets of human demonstrations collected with a Virtual Reality (VR) headset and a motion capture glove. While collecting demonstrations in this setup can provide accurate state-action trajectories for behavior cloning, the data collection process is high-cost and not scalable. There are only 25

* Equal Contribution

demonstrations collected for each task. The way the demonstration is collected also limits the complexity of the task: RL can achieve similar performance with or without using the demonstrations in most tasks [57]. With these observations, we argue it is critical to increasing the difficulty and complexity of the manipulation tasks with diverse daily objects for real world applications. At the same time, solving these tasks under different configurations will require large-scale human demonstrations which are hard to obtain with VR but are much more available from human videos.

In this paper, we propose **a new platform and a new imitation learning pipeline** for complex and generalizable dexterous manipulation, namely DexMV (**D**exterous **M**anipulation from **V**ideos). We introduce new tasks with the multi-finger robot hand (Adroit Robotic Hand [39]) on diverse objects in simulation. We collect real human hand videos performing the same tasks as demonstrations. By using human videos instead of VR, it *largely reduces the cost* for data collection and allows humans to perform more *complex and diverse* tasks. While the video demonstrations might not be optimal for perfect imitation (e.g., behavior cloning) to learn successful policies, the diverse dataset is beneficial for augmenting the training data for RL, which can learn from both successful and unsuccessful trials.

Our DexMV platform contains a paired systems with: (i) A computer vision system which records the videos of human performing dexterous manipulation tasks (1st row in Figure 1); (ii) A physical simulation system which provides the interactive environments for dexterous manipulation tasks with a multi-finger robot hand (3rd row in Figure 1). The two systems are aligned with the same manipulation tasks with multi-finger hands. With this platform, our goal is to bridge computer vision and robotic dexterous manipulation via a new imitation learning pipeline.

Our DexMV pipeline contains three stages. First, given the recorded videos from our computer vision system, we extract the 3D hand-object poses from the videos (2nd row in Figure 1). Unlike previous imitation learning studies with 2-DoF grippers [86, 75], we need the human video to guide the 30-DoF robot hand to move each finger in 3D space. Parsing the 3D structure provides critical and necessary information. Second, we perform motion retargeting which converts the 3D human hand trajectories to robot hand trajectories. An optimization-based approach is proposed to align human-robot hands under kinematic constraints. Third, given the robot demonstrations, we perform imitation learning in the simulation tasks. We investigate algorithms which augment RL objectives with state-only [57] and state-action [28, 59] demonstrations. While each individual component is built on existing work, *our pipeline connecting 3D vision to imitation learning with our systems has not been studied before.*

We experiment with three types of challenging tasks with

the YCB objects [15]. The first task is to *relocate* an object to a goal position. Instead of relocating a single ball as [59], we increase the task difficulty by using diverse objects (first 5 columns in Figure 1). The second task is *pour*, which requires the robot to pour the particles from a mug into a container (Figure 1 from column 6). The third task is *place inside*, where the robot hand needs to place an object into a container (last 2 columns in Figure 1). It requires manipulation of both the position and the orientation of the object. In our experiments, we benchmark different imitation learning algorithms and show human demonstrations indeed can improve dexterous hand manipulation by a large margin. We elaborate how the number of demonstrations and the quality of pose estimation can affect imitation learning, and how demonstrations can be transferred to environments with different physical parameters and different objects. We hope our new platform and pipeline open up opportunities for research that connects imitation learning and 3D vision.

2. Related Work

Dexterous Manipulation. Manipulation with multi-finger hands is one of the most challenging core robotics tasks, which has been actively studied with optimization and planning [63, 9, 46, 18, 2, 6]. Recently, researchers have started exploring reinforcement learning for dexterous manipulation and show the learned policy can be transferred to the real robot hand [48, 47]. However, training with only RL requires a large number of samples. Different from a regular 2-DoF robot gripper, the Adroit Robotic Hand has 24 joints, which greatly increases the optimization space. The most challenging task in [59] is relocating a ball, which is hard to be solved without using the demonstrations. In this paper, we replace the ball with daily objects in the *relocate* task, which makes the task even harder.

Imitation Learning from Human Demonstrations. Imitation learning from expert demonstrations has shown promising results in improving the sample efficiency over RL. The way to perform imitation learning is not limited to behavior cloning [54, 7, 62, 10, 82], but also via inverse reinforcement learning (IRL) [64, 45, 1, 28, 20, 4, 83, 41] and augmenting the RL training data with demonstrations [53, 19, 84, 59, 57]. For example, Rajeswaran *et al.* [59] propose to incorporate demonstrations with on-policy RL with an auxiliary term. However, all these approaches rely on expert demonstrations in state space collected using expert policies or VR, which is not scalable and generalizable to complex tasks. In fact, it is shown in [57] that RL can achieve similar performance and sample efficiency with or without the demonstrations in most dexterous manipulation tasks in [59] besides *relocate*. To conquer this problem, researchers have recently looked into imitation learning and RL with videos [66, 16, 65, 70, 75, 86]. For example, Schmeckpeper *et al.* [65] collect human videos on manip-

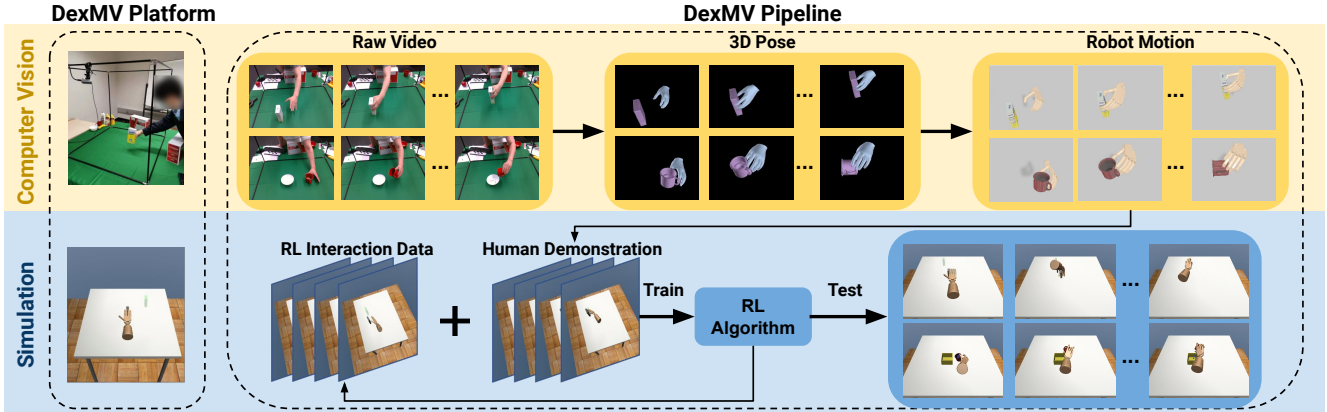


Figure 2: **DexMV platform and pipeline overview.** Our platform is composed of a computer vision system (colored with yellow) and a simulation system (colored with blue). In our computer vision system on top, we collect human videos of dexterous manipulation tasks. In the simulation system at the bottom, we design the same manipulation tasks for the robot hand. In the DexMV pipeline, we apply 3D hand and object pose estimation from the videos, followed by hand motion retargeting to generate robot hand demonstrations. We then adopt the imitation data to augment reinforcement learning with three different algorithms.

ulation tasks for scaling up learning. However, the tasks are relatively simple (e.g., pushing a block) with a 2-jaw parallel gripper. In this paper, we propose new challenging dexterous manipulation tasks. Under these tasks, we show accurate 3D pose estimation becomes necessary for providing demonstrations that largely improve imitation learning performance while using RL alone fails to solve these tasks.

Following Human Demonstrations. Another line of work in imitation learning is to train policies to follow the expert demonstrations [43, 52, 49, 71, 68, 72, 74, 21, 51, 73]. For example, Garcia-Hernando *et al.* [21] propose to use RL to map an estimated hand pose from a user RGB-D image to a virtual robot hand. The robot hand can execute the same trajectory by following the human hand videos. Instead of repeating one expert trajectory, we emphasize that DexMV is about learning a policy that can be generalized to different goals, object arrangements, and configurations.

Hand-Object Interaction. Hand-object interaction has been widely studied in computer vision. One line of work focus on object pose estimation [36, 56, 85, 79, 50, 30, 27] and hand pose estimation [87, 31, 76, 23, 5, 11, 26, 38, 42]. Berk *et al.* [15] propose the YCB dataset with real objects and their 3D scans. Xiang *et al.* [85] further extend this dataset with 6D pose annotations. Beyond object poses, datasets for joint estimation of the object and hand poses are also proposed [22, 88, 24, 42]. Another line of datasets focus on hand-object contact reasoning [12, 17, 78, 14]. For example, Brahmabhatt *et al.* [12] propose to collect the contact maps on objects with a thermal camera, which can be used to learn functional grasps [32, 13, 44]. In this paper, we collect paired human videos in the real world for different robot hand manipulation tasks in simulation. We perform imitation learning for these tasks, which at the same time provides a new way for hand-object interaction reasoning.

3. Overview

We propose DexMV for **Dexterous Manipulation** with imitation learning from human **Videos**, which contains two main components:

(i) **DexMV platform**, which offers a paired computer vision system recording human manipulation videos and physical simulators conducting the same tasks. We design three challenging dexterous manipulation tasks in the simulation system, and the computer vision system is used to collect the human demonstrations to help solve these tasks. The human videos can be efficiently collected with around *100 demonstrations per hour*.

(ii) **DexMV pipeline**, a new pipeline for imitation learning from human videos. Given the recorded videos from the computer vision system, we perform 3D hand-object pose estimation and motion re-targeting to convert human hand trajectories to robot hand demonstrations. These demonstrations are then used for policy learning where multiple imitation learning and RL algorithms are investigated under our pipeline. By learning from multiple demonstrations, our policy can be deployed in environments with *different goals and object configurations*, instead of just following one trajectory. We show that given the complex manipulation tasks, 3D pose estimation provides *necessary signals* for imitation learning to learn successful and natural policies.

We will introduce the DexMV platform in Section 4 and then the DexMV pipeline in Section 5.

4. DexMV Platform

We illustrate our DexMV platform in Figure 2. It is composed of a computer vision system and a simulation system. We will introduce both systems in the following.

4.1. Computer Vision System

The computer vision system is used to collect human demonstration videos on manipulating diverse real objects. In this system, we build a cubic frame (35 inch³) and attach two RealSense D435 cameras on the top front and top left of the frame. During data collection, a human will perform manipulation tasks inside the frame, e.g., relocate sugar box. The manipulation videos will be recorded using the two cameras (from a front view and a side view). The computer vision system is shown on the top row of Figure 2. The collected videos will then be the input of our DexMV pipeline to learn manipulation skills of a multi-finger robot hand.

4.2. Simulation System

Our simulation system is built on MuJoCo [80] with the Adroit Hand [39]. We design multiple dexterous manipulation tasks aligned with human demonstrations. As shown in the bottom row of Figure 2, we perform imitation learning by augmenting the Reinforcement Learning objective with the demonstrations from the computer vision system. Once the policy is trained, it can be tested on achieving manipulation tasks under different goals and object configurations. We will introduce the imitation learning algorithms in detail in Section 5.4.

4.3. Task Description

We propose three types of manipulation tasks with different objects. We select the objects which have a reasonable size and easy for human to manipulate from the YCB datasets [15]. The number of human demonstrations col-

Task	#Demo
Relocate	
+ Mug	100
+ SugarBox	100
+ LargeClamp	100
+ TomatoSoup	100
+ MustardBottle	100
Pour	100
Place Inside	100

lected for each task is shown in the right table. More details on task and environment can be found in Supplementary Section C.

Relocate. This task requires the robot hand to pick up an object on the table to a target location. It is inspired by the hardest task in [59] where the robot hand needs to grasp a sphere and move it to the target position. We further increase the task difficulty by using 5 complex and diverse objects including mug, mustard bottle, sugar box, tomato soup can, and large clamp. We visualize the tasks in the first 5 columns of Figure 1. The transparent green shape represents the goal location, which can change during policy training and testing for each episode (goal-conditioned). The task is successfully solved if the object reaches the goal, and it does not need to be placed in a specific orientation. We train one policy for relocating each object.

Pour. This task requires the robot hand to reach the mug and pour the particles inside the mug into a container as

shown in Figure 1 column 6. The reward will be higher with more particles poured into the container. This task is much more challenging than relocate as it not only requires grasping the mug but also manipulate it in a delicate way to pour the particles precisely into the container. The evaluation for this task is based on how much percentage of the particles are pulled inside the container.

Place Inside. This task requires the robot hand to pick up an object (i.e., a banana in our task) on the table and place it into a container. It is much more challenging than relocate since the robot needs to rotate the object to a suitable orientation with finger gait. Besides, when approaching the container, the robot needs to carefully avoid collisions between both hand-container pair and object-container pair. The evaluation for this task is based on how much percentage of the object mesh volume is inside the container. We will introduce the rewards for all tasks in the supplementary materials.

5. DexMV Pipeline

We propose a novel imitation learning pipeline based on the introduced platform. Our DexMV pipeline takes as input the human demonstration video collected in the computer vision system and learns dexterous manipulation skills for a multi-finger robot hand in simulation. The DexMV pipeline contains three stages: (i) 3D hand-object pose estimation from videos, described in Section 5.1 and Section 5.2; (ii) Hand motion retargeting to convert human hand motion into robot motor command, described in Section 5.3; (iii) Imitation learning in the simulation environment given robot demonstration from retargeting, which will be described in Section 5.4.

Unlike previous imitation learning studies with 2-DoF grippers, the DexMV pipeline provides a comprehensive approach to learn manipulation skills for 30-DoF robot hand with a much larger action space. We emphasize that to solve such a complex task, 3D information from the demonstration becomes necessary. The proposed pipeline provides a general approach for learning dexterous manipulation from human video and is extendable to other tasks beyond the current three tasks.

5.1. Object Pose Estimation

We use the 6-DoF pose to represent the location and orientation of objects, which contains translation $T \in \mathbf{R}^3$ and rotation $R \in \mathbf{SO}(3)$. For each frame t in the video, we use the PVN3D [27] model trained on the YCB dataset [15] to detect objects and estimate their 6-DoF poses. By taking both the RGB image and the point clouds deprojected from the depth image as inputs, the model first estimates the instance segmentation mask. With dense voting on the segmented point clouds, the model then predicts the 3D location of pre-defined object keypoints. More specifically,

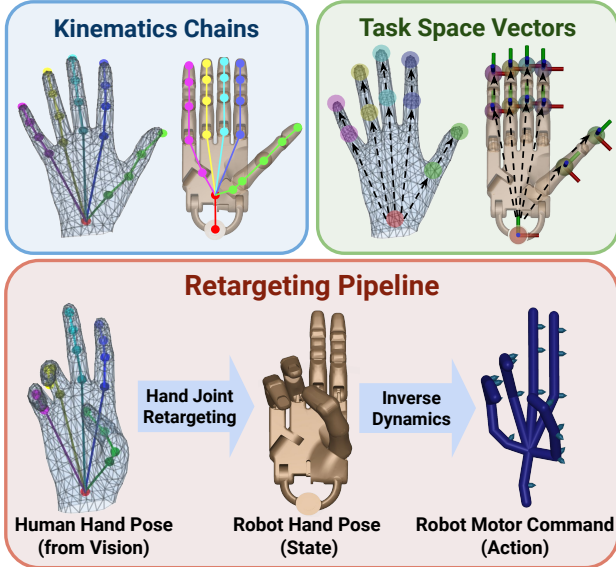


Figure 3: **Top row:** Kinematic Chains and Task Space Vectors (TSV) of human and robot hand. The TSV (shown in dash arrows) are ten vectors to be matched between both hands. **Bottom row:** Two steps of hand motion retargeting: (i) Optimize the robot TSV to match human TSV and generate the robot joint trajectory (state in demonstrations); (ii) Use inverse dynamics to compute the robot motor command (action in demonstrations).

the 6-DoF object pose can be optimized by minimizing the following PnP matching error,

$$E_{match} = \sum_{i=1}^K \|\hat{k}p_t^i - (R_t \cdot kp^i + T_t)\|_2^2, \quad (1)$$

where K is the number of object keypoints, $\hat{k}p_t^i$ is the predicted i^{th} keypoint of frame t , and kp^i is its counterpart in the object local coordinate. We estimate the object pose using a single camera from the front view, which matches the object views where the PVN3D model is trained on.

5.2. Hand Pose Estimation

We utilize the parametric MANO model [61] to represent the hand in a differentiable manner, which consists of hand pose parameter θ_t for 3D rotations of 15 joints and root global translation, roots global rotation r_t , and shape parameters β_t for each frame t . The output 3D hand joints can be computed using the forward kinematics function $j_t^{3d} = \mathcal{J}(\theta_t, \beta_t, r_t)$.

Given a video, we use the off-the-shelf skin segmentation [37] and hand detection [69] models to obtain a hand mask M_t for every frame t . We use the trained hand pose estimation models in [42] to predict the 2D hand joints j_t^{2d} and the MANO parameters θ_t and β_t for every frame t in the captured sequence using the RGB inputs. We estimate the root joint r_t using the center of the depth image masked

by segmentation M_t . Given the initial estimation θ_t, β_t, r_t of each frame t and the camera pose Π , we formulate the 3D hand joint estimation as an optimization problem,

$$\theta_t^*, \beta_t^*, r_t^* = \arg \min_{\theta_t, \beta_t, r_t} E_{2d} + \lambda E_{depth}, \quad (2)$$

$$E_{2d} = \|\Pi J(\theta_t, \beta_t, r_t) - j_t^{2d}\|^2,$$

$$E_{depth} = \|M_t \cdot (\mathcal{R}(\theta_t, \beta_t, r_t) - D_t)\|^2,$$

where $\lambda = 0.001$ and \mathcal{R} is a depth rendering function [35] and D_t is the corresponding depth map in frame t . We use E_{2d} to minimize the re-projection error in 2D and E_{depth} to obtain the hand 3D locations from the depth map. While Equation 2 is designed for a single camera, it can be easily extended to a multi-camera setting by minimizing the errors E_{2d} and E_{depth} from different cameras with known extrinsics. We perform our experiments using two cameras by default to handle occlusion. We will ablate how the number of cameras affects policy performance.

Besides the pose estimation model, we add a post-processing procedure for temporal smoothness and shape consistency by minimizing the following error:

$$E_{post} = \sum_{t=1}^{N-1} \|j_{t+1}^{3d} - j_t^{3d}\|^2 + \sum_{t=1}^N \|\beta_t - \bar{\beta}\|^2, \quad (3)$$

where N is the number of frames and $\bar{\beta}$ is the average shape prediction of the sequence. The first term in Equation 3 is to improve the temporal smoothness of the hand joints and the second term penalizes the shape variation over time.

5.3. Hand Motion Retargeting

To use the human demonstrations in our simulator, we need to convert the human hand motion to robot hand motion. Human and robot hands are intrinsically different, although they share a similar five-finger morphology. The MANO model [61] for the human hand is composed of 15 ball joints with 45 DoF. The Adroit Robotic Hand [39] used in our experiments is actuated by 24 revolute joints with 24 DoF. In addition, the length of each knuckle between robot hand and human hand is not the same, which also brings the discrepancy between the two hands. The two hands are shown in Figure 3. To bridge the gap between these two models, Hand Motion Retargeting, also called Kinematics Retargeting [25] or Teleportation Mapping [40, 60], can be used to map the observed human hand pose to the robot hand joints. There are two steps in motion retargeting in our pipeline: (i) hand joint retargeting which generates state-only demonstration and (ii) inverse dynamics which generates state-action demonstration.

Hand joint retargeting. Our hand joint retargeting approach is inspired by [3, 25]. The initial guess of the robot hand pose is computed via a fitness function, which converts the human hand pose to robot joint configuration using linear mapping. Given this initial guess, we perform



Figure 4: Visualization of hand motion retargeting results. **Top row:** Object and hand pose estimation results. **Bottom row:** Robot hand pose after hand motion retargeting module.

another optimization approach via task space vectors. Different from the commonly used fingertip mapping [25, 60], we also include the proximal phalanx into the objective shown in Figure 3. During optimization, we minimize the difference of ten task space vectors: vectors from wrist to proximal phalanx plus vectors from proximal phalanx to tip for all five fingers. Here we use Sequential Least-Squares Quadratic Programming implemented in NLOpt [33] library as the optimization algorithm. Please refer to the supplementary materials for more details. Example results of hand joint retargeting are shown in Figure 4. Combining the object pose and the joint retargeting results, we obtain the state-only demonstrations for imitation learning.

Inverse dynamics. In our manipulation tasks, the action is defined as the actuation of the robot finger motor. To generate the action for state-action demonstrations, we first fit the hand pose sequence with min-jerk cubic spline model [81] for time parameterization. Then velocity and acceleration can be computed by taking the derivative of the fitted function. After that, we can compute the torque with robot inverse dynamics based on the position, velocity, and acceleration. The torque is defined in the generalized coordinates. The last step is to convert the joint torque into motor actuation, which is the action space in the simulated environment. Since we use the position servo in MuJoCo, the actuation is a linear mapping of torque and current joint position for each frame. More details on demonstration generation can be found in Supplementary Section D.

5.4. Imitation Learning

We perform imitation learning using the demonstrations generated from our computer vision system. Instead of using behavior cloning, we adopt imitation learning algorithms which incorporate the demonstrations into RL. In this section, we will first introduce the RL background, and then the imitation learning methods using state-action demonstrations [29, 58] and state-only demonstrations [57].

Reinforcement Learning background. We consider the standard Markov Decision Process (MDP) [77]. It is represented by a tuple $\langle S, \mathcal{A}, \mathcal{P}, \mathcal{R}, \gamma \rangle$, where S and \mathcal{A} are state and action space, $\mathcal{P}(s_{t+1}|s_t, a_t)$ is the transition density of state s_{t+1} at step $t + 1$ given action a_t made under state

s_t , $\mathcal{R}(s, a)$ is the reward function, and γ is the discount factor. The goal of RL [77] is to maximize the expected reward with a stochastic policy $\pi(a|s)$. Occupancy measure ρ_π [55] is a density measure of the state-action tuple on policy π as shown below:

$$\rho_\pi(s, a) = \pi(a|s) \sum_{t=0}^{\infty} \gamma^t \Pr(s_t = s | \pi),$$

where $\Pr(s_t = s | \pi)$ is the probability density of state s at time step t following policy π . The occupancy measure plays an important role in IL literature because of its one-to-one correspondence with the policy. The correspondence provides a possible direction to learning from demonstrations since the expert policy generating the given demonstration can be recovered by matching the distribution of the demonstrations.

Imitation Learning algorithms. When facing complex tasks like dexterous manipulation, RL suffers from poor sample complexity and it often leads to unnatural behaviors. To alleviate this challenge, we incorporate reinforcement learning with imitation learning. Given trajectories $\{(s_i, a_i)\}_{i=1}^n$ generated by an expert π_E , we optimize the agent policy π_θ to recover the expert policy π_E with $\{(s_i, a_i)\}_{i=1}^n$ and reward function \mathcal{R} .

In this paper, we evaluate the performance of three imitation learning methods under two settings: state-action imitation learning and state-only imitation learning. All methods utilize both expert demonstrations and a reward function to learn the dexterous manipulation tasks. That is, the imitation learning algorithms here provide different ways to incorporate the expert demonstrations with Reinforcement Learning. For fair comparison, we adopt the *same RL algorithm* for all methods.

State-action imitation learning. We will introduce two algorithms. The first one is the Generative Adversarial Imitation Learning (GAIL) [29], which is the SOTA IL method that performs occupancy measure matching to learn parameterized policy. Occupancy measure matching aims to minimize the objective $d(\rho_{\pi_E}, \rho_{\pi_\theta})$, where d is a distance function, π_θ is a policy to be learned and parameterized by θ . The key idea behind GAIL is that it uses generative adversarial training to estimate the distance and minimize it alternatively. This leads to the following min-max optimization problem:

$$\min_{\theta} \max_w \mathbb{E}_{s, a \sim \rho_{\pi_\theta}} [\log D_w(s, a)] + \mathbb{E}_{s, a \sim \rho_{\pi_E}} [\log(1 - D_w(s, a))]$$

where D_w is a discriminator parameterized by w . To equip GAIL with reward function, we adopt the approach proposed by [34], which combines the discriminator feedback and reward signal via reward shaping. In the following context, we denote this method as GAIL+.

The second algorithm is Demo Augmented Policy Gradient (DAPG) [58]. It combines learning from demonstration and policy optimization for better sample complexity and resulting policies. The objective function for policy optimization at each iteration k can be represented as,

$$g_{aug} = \sum_{(s,a) \in \rho_{\pi_{\theta}}} \nabla_{\theta} \ln \pi_{\theta}(a|s) A^{\pi_{\theta}}(s, a) + \sum_{(s,a) \in \rho_{\pi_E}} \nabla_{\theta} \ln \pi_{\theta}(a|s) \lambda_0 \lambda_1^k \max_{(s',a') \in \rho_{\pi_{\theta}}} A^{\pi_{\theta}}(s', a'),$$

where $A^{\pi_{\theta}}$ the advantage function [8] of policy π_{θ} , and λ_0 and λ_1 hyper-parameters bounded by 0 and 1.

State-only imitation learning. While state-action imitation approaches are shown to be effective, the action information computed from our motion retargeting approach might not be ideal. Thus we also investigate the demonstration with State-Only Imitation Learning (SOIL) [57], which extends DAPG to the state-only imitation setting and addresses the challenge by learning an inverse dynamics model h_{ϕ} optimizing the objective with the collected trajectories when running the policy,

$$L_{mse} = \sum_{(s_t, a_t, s_{t+1}) \in \rho_{\phi_{\theta}}} \|a_t - h_{\phi}(s_t, s_{t+1})\|^2.$$

The inverse dynamics model is then used to predict the missing actions in state-only demonstrations and then train the policy using state-action demonstrations as DAPG. The policy and the inverse dynamics model are optimized simultaneously during training.

6. Experiment

We conduct experiments on the proposed tasks including *Relocate* five different objects, *Pour* and *Place Inside* defined in Section 4.3. We adopt our DexMV pipeline, and benchmark different imitation learning algorithms on these tasks. We ablate how different ways for hand pose estimation, number of demonstrations, and different environmental parameters can affect imitation learning.

Experiment and comparison settings. We adopt TRPO [67] as our Reinforcement Learning baseline. We benchmark imitation learning algorithms including SOIL, GAIL+, and DAPG as introduced in Section 5.4. All these imitation learning algorithms incorporate the demonstrations with the same RL algorithm (TRPO) using the same hyper-parameters. Thus all the algorithms we tested are comparable. We parameterized the policy and value function with two separate 2-layer MLPs. For each update iteration, we collect 200 trajectories from the environments to estimate the policy gradient and update both policy and value networks. In all experiments, the performance is evaluated with three individual random seeds and the seeds are the same across all comparisons.

The hand pose in the demonstrations is estimated using two cameras with post-processing as default for all approaches. For the state-action imitation baselines that require action information such as GAIL+ and DAPG, we use inverse dynamic (Section 5.3) to compute the robot action.

6.1. Experiments with Relocate

Main comparisons. We evaluate and benchmark four methods: SOIL, GAIL+, DAPG, and RL on the *Relocate* tasks. The results is presented in terms of *success rate* in Table 1 and training curve in Figure 5. A trial is counted as success only when the final position of the object (after executing the policy for 200 steps) is within 0.1 unit length to the specified target. Note that both the initial object position and target position are randomized for each episode. Figure 5 shows the average reward by three policies trained with different seeds. The x-axis is the update iterations during training and the average-return of y-axis is normalized to the same range for all five relocate tasks.

Both Table 1 and Figure 5 show that the imitation learning methods can outperform the RL baseline for all five tasks. For relocating mustard bottle and sugar box, a pure RL agent cannot learn anything without the help of human demonstrations. For sugar box and large clamp, SOIL can performs the best while DAPG achieves the comparable or better performance on mug, mustard bottle, and tomato soup can. The difference between state-only and state-action imitation learning is caused by the different ways the action is computed. For using the inverse dynamics method analytically during motion retargeting, we clip the motor command between the lower and upper limit of action space. When computing action for sugar box (which is relatively heavy), the computed motor command often gets out of the limits, which hurts the quality of the action and affects imitation learning performance for DAPG and GAIL+. Instead of computing the action analytically, SOIL learns the inverse dynamics model to estimate the action online during training, which allows for more flexibility.

Ablation on hand pose estimation. To investigate the relationship between perception module and imitation learning module, we choose 4 different settings for hand pose estimation from video captured by: (i) single camera; (ii) single camera plus post-processing (iii) dual camera; (iv) dual cameras plus the post-processing (Equation 3, which is applied by default in other experiments). The object pose is the same across 4 settings. We train imitation learning agents with these four different demonstrations using SOIL on the relocate task with a tomato soup can. As shown in Figure 6 (a), we find more advanced techniques for hand pose estimation leads to better imitation learning performance, and the demonstration generated with dual-camera plus post-processing achieves the best results. This indicates the potential of using our manipulation task as

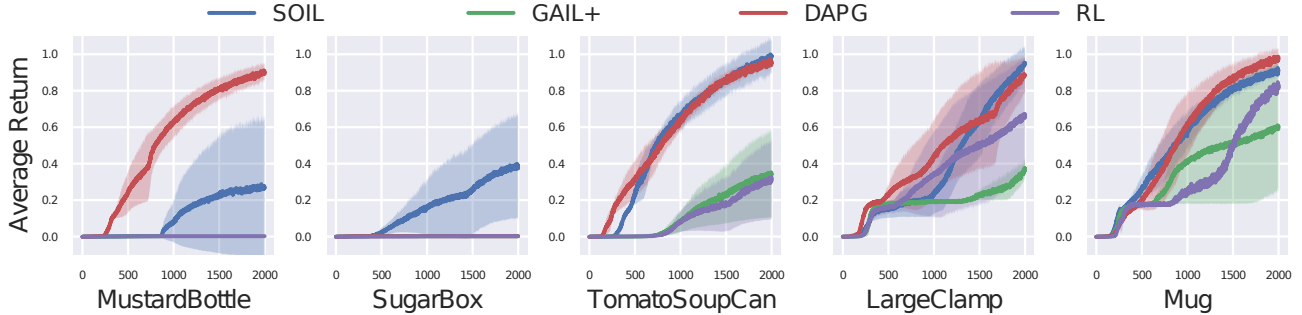


Figure 5: Learning curves of the four methods on the relocate task with respect to five different objects. The x-axis is training iterations. The shaded area indicates standard error and the performance is evaluated with three individual random seeds.

Model	Task - Relocate				
	Mustard Bottle	Sugar Box	Tomato Soup Can	Large Clamp	Mug
SOIL	0.33 ± 0.42	0.67 ± 0.47	0.98 ± 0.02	0.89 ± 0.15	0.71 ± 0.35
GAIL+	0.06 ± 0.01	0.00 ± 0.00	0.66 ± 0.47	0.52 ± 0.39	0.53 ± 0.37
DAPG	0.93 ± 0.05	0.00 ± 0.00	1.00 ± 0.00	1.00 ± 0.00	1.00 ± 0.00
RL	0.06 ± 0.01	0.00 ± 0.00	0.67 ± 0.47	0.51 ± 0.37	0.49 ± 0.36

Table 1: Success rate of the evaluated methods on the relocate task with five different objects. The success is defined based on the distance between object and target. The performance is evaluated via 100 trials for three seeds.

Model (#Demo)	Iterations		
	400	600	800
SOIL (100)	0.36 ± 0.13	0.70 ± 0.25	1.00 ± 0.00
SOIL (50)	0.19 ± 0.23	0.40 ± 0.43	0.59 ± 0.39
SOIL (10)	0.04 ± 0.05	0.17 ± 0.11	0.36 ± 0.21
RL	0.00 ± 0.00	0.00 ± 0.00	0.13 ± 0.19

Table 2: Success rate of SOIL with different number of demonstrations on the relocate task with tomato soup can. The performance is evaluated via 100 trials for three seeds.

one downstream metric to evaluate the quality of pose estimation. *How good a pose estimator is should not only be judged by the distance from the GT keypoints, but rather could be how much it can help imitation learning.*

Ablation on the number of demonstrations. Figure 6 (b) shows the performance of SOIL with respect to different number of demonstrations. We use the relocate with a tomato soup can. We observe that SOIL can achieve better sample efficiency and performance when more demonstrations are given. By rendering and observing the failure cases, we find reaching and grasping the objects are two critical bottlenecks for the RL baseline. The given demonstrations help SOIL to conquer these challenges with much fewer training samples. Table 2 further illustrates the success rate of the different policies (trained with different number of demonstrations) across iterations. Specifically, at iteration 400, SOIL trained with 100 demonstrations can reach an average success rate of 83%, better than training with 10 demonstrations (60%). In comparison, pure RL only achieves 13% success rate.

More demonstrations also reduce the variance. We observe that SOIL with 100 demonstrations achieve much smaller variance from Table 2 and a smaller shaded area in training curve in Figure 6 (b). *This ablation study shows the importance of finding an efficient way to scale up the number and diversity of demonstrations using our pipeline.*

Ablation on environmental conditions. Figure 6 (c) and (d) illustrates that our demonstrations can transfer to different physical environments. Given the same demonstrations on *Relocate* the tomato soup can, we train policies with scaling the object sizes into different scales from

$\times 0.75$ to $\times 1.125$ (Figure 6 (c)) and applying different scales of frictions (Figure 6 (d)) from $\times 0.8$ to $\times 1.2$. With the same demonstrations, we can still transfer and utilize them to perform imitation learning in these different environments, and achieve relatively consistent results. Note that all the policies achieve much better performance than pure RL. *This experiment shows the robustness of our pipeline against the gap between simulation (environment) and real (demonstration).*

Ablation on transferring across objects. We investigate whether the demonstration can still help when we change the object to manipulate when training the policy. For example, the first curve in Figure 7 shows the rewards on training a policy to relocate a potted-meat-can while still using demonstration on relocating tomato soup can. As the two objects have similar sizes, we find using imitation learning with SOIL continues to achieve much better results than pure RL. We also observe improvements when training to relocate foam brick using the demonstration of sugar box (2nd curve in Figure 7). However, when the two objects have large differences in size and geometric shape like between the mug and the bowl, imitation learning stops helping (3rd curve in Figure 7). *This experiment shows while our pipeline is robust and can generalize to similar objects, accurate capture of 3D still matters.*

6.2. Experiments with Pour

The *Pour* task involves a sequence of dexterous manipulations: reaching the mug, holding the mug, stably moving the mug, and pouring water into the container without squirting. We report our results in Figure 8. We observe that DAPG converges to a good policy with much fewer itera-

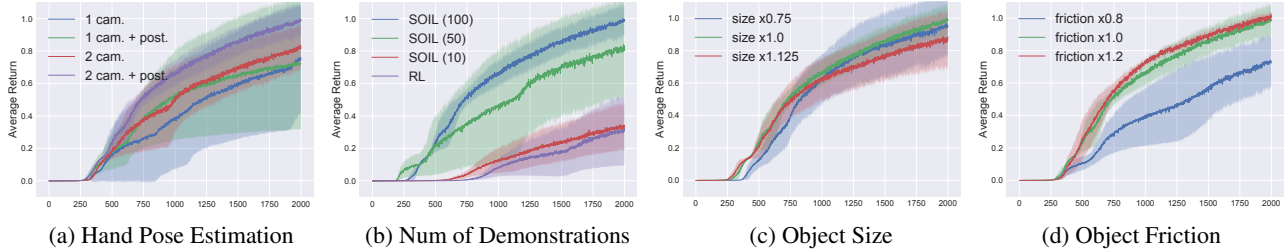


Figure 6: **Ablation Study:** Learning curves of SOIL on the *Relocate* task with tomato soup can. From left to right, we performance ablation study on: hand pose estimation settings, number of demonstrations used to train SOIL, scaling of object size, and friction parameter of the relocated object. Note that for object size ablation and friction ablation, the demonstrations are kept same for all conditions.

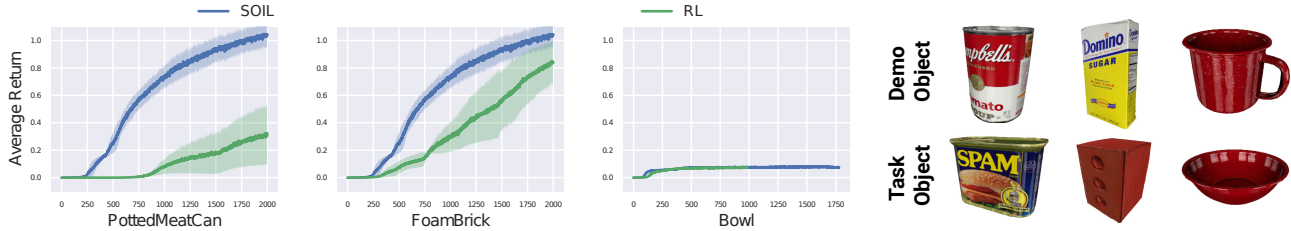


Figure 7: Object transfer on the *Relocate* task. An imitation learning agent is trained with demonstrations on the original demo object, e.g. tomato soup can (first row of right figure), to relocate a novel object, e.g. potted meat can (second row of right figure).

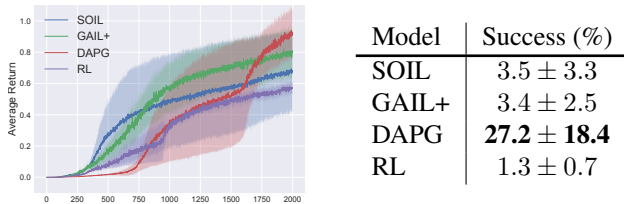


Figure 8: Evaluation on the *Pour* task. The right table shows the success rate, which is computed based on the percentage of water particles poured into the container. The left figure shows the learning curve of different method.

tions: 27 % of the particles are poured into the container on average. Other imitation approaches only perform slightly better than pure RL. Without the demonstrations, pure RL will only have a very small chance to pour few particles into the container. Unlike *Relocate*, state-action method DAPG performs much better than state-only method SOIL in this task. This is due to it is very challenging to learn a good inverse model with the existence of water particles in this task for state-only method SOIL. In contrast, although the contact force is not perfect for the action computed from analytical inverse dynamics function, it still boosts the performance for DAPG.

Visualization on naturalness. We execute the policies and visualize a successful trial of DAPG and a relatively successful RL trial (which is rare) in Figure 9. We can obtain different results because the location of the mug is randomized. We show that DAPG learns to naturally hold the mug and pour the particles into the container. But the RL policy tries to utilize its wrist and the edge of the container

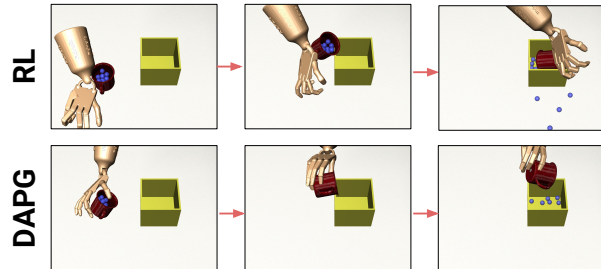


Figure 9: Comparison of the naturalness on the *Pour* task between **Top Row:** policy learned by TRPO without demonstrations; **Bottom Row:** policy learned by DAPG with demonstrations.

to flip the mug for pouring, which rarely succeeds. These results emphasize the importance of learning from human demonstrations since learning an unexpected policy can be dangerous in real-world applications.

6.3. Experiments with Place Inside

The *Place Inside* task requires the robot hand to first pick up a banana, rotate it to the appropriate orientation, and then place it inside of the mug. To measure the final performance of this task, we define a metric called *Inside Score*, which is computed based on the volume percentage of banana inside of the mug (the volume inside the mug divided by the whole volume of the banana). Since the banana is longer than the mug, the volume percentage of banana inside can never reach 100%. To normalize this score, we first measure the maximum possible volume of the banana that can be inside of the mug, which is 78.19%. Then we divide the inside volume percentage by this maximum possible volume percentage to compute the *Inside Score*.

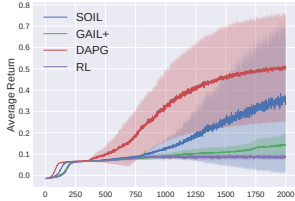


Figure 10: Evaluation on the *Place Inside* task. The right table shows the inside score, which is based on the volume of banana inside of the mug. The left figure shows the learning curve of different method.

We present our results in Figure 10, we find that DAPG outperforms other approaches whereas RL hardly learns to manipulate the object. This task is much more challenging than *Relocate* since the robot hand needs to learn a delicate finger gait to reorient the object while keeping the banana and the outside edge of the container from collision. Between state-only method (SOIL) and state-action method (DAPG), we again observe that computing action offline analytically achieves better results, due to the complexity of the task.

7. Conclusion

To the best of our knowledge, DexMV is the first work to provide a platform on computer vision/simulation systems and a pipeline on learning dexterous manipulation tasks from human videos. DexMV platform contains a simulation system for complex dexterous manipulation tasks and a computer vision system to record corresponding human demonstrations. This platform allows for efficient, large-scale and diverse demonstration collection (100 demonstrations per hour), which we show in our experiments are very important to improve learning. Our DexMV pipeline connects from 3D pose estimation and imitation learning. We benchmark with multiple imitation learning algorithms in our experiments and review the effectiveness and robustness of our pipeline. Importantly, we study on how computer vision estimation results can affect imitation learning. We hope this opens up new research opportunities for not only robot learning but also computer vision to evaluate and benchmark vision algorithms using our downstream tasks.

References

[1] Pieter Abbeel and Andrew Y Ng. Apprenticeship learning via inverse reinforcement learning. 2004. 2

[2] Sheldon Andrews and Paul G Kry. Goal directed multi-finger manipulation: Control policies and analysis. *Computers & Graphics*, 2013. 2

[3] Dafni Antotsiou, Guillermo Garcia-Hernando, and Tae-Kyun Kim. Task-oriented hand motion retargeting for dexterous manipulation imitation. In *Proceedings of the European*

Conference on Computer Vision (ECCV) Workshops, pages 0–0, 2018. 5

[4] Yusuf Aytar, Tobias Pfaff, David Budden, Thomas Paine, Ziyu Wang, and Nando de Freitas. Playing hard exploration games by watching youtube. In *NeurIPS*, 2018. 2

[5] Seungryul Baek, Kwang In Kim, and Tae-Kyun Kim. Pushing the envelope for rgb-based dense 3d hand pose estimation via neural rendering. In *CVPR*, pages 1067–1076, 2019. 3

[6] Yunfei Bai and C Karen Liu. Dexterous manipulation using both palm and fingers. 2014. 2

[7] Michael Bain and Claude Sammut. A framework for behavioural cloning. In *Machine Intelligence 15*, 1995. 2

[8] Leemon C Baird III. Advantage updating. Technical report, WRIGHT LAB WRIGHT-PATTERSON AFB OH, 1993. 7

[9] Antonio Bicchi. Hands for dexterous manipulation and robust grasping: A difficult road toward simplicity. *IEEE Transactions on robotics and automation*, 16(6):652–662, 2000. 2

[10] Mariusz Bojarski, Davide Del Testa, Daniel Dworakowski, Bernhard Firner, Beat Flepp, Prasoon Goyal, Lawrence D Jackel, Mathew Monfort, Urs Muller, Jiakai Zhang, et al. End to end learning for self-driving cars. *arXiv*, 2016. 2

[11] Adnane Boukhayma, Rodrigo de Bem, and Philip HS Torr. 3d hand shape and pose from images in the wild. In *CVPR*, pages 10843–10852, 2019. 3

[12] Samarth Brahmabhatt, Cusuh Ham, Charles C Kemp, and James Hays. Contactdb: Analyzing and predicting grasp contact via thermal imaging. In *Proceedings of the IEEE/CVF Conference on Computer Vision and Pattern Recognition*, pages 8709–8719, 2019. 1, 3

[13] Samarth Brahmabhatt, Ankur Handa, James Hays, and Dieter Fox. Contactgrasp: Functional multi-finger grasp synthesis from contact. *arXiv preprint arXiv:1904.03754*, 2019. 3

[14] Samarth Brahmabhatt, Chengcheng Tang, Christopher D Twigg, Charles C Kemp, and James Hays. Contactpose: A dataset of grasps with object contact and hand pose. *arXiv preprint arXiv:2007.09545*, 2020. 3

[15] Berk Calli, Aaron Walsman, Arjun Singh, Siddhartha Srinivasa, Pieter Abbeel, and Aaron M Dollar. Benchmarking in manipulation research: The ycb object and model set and benchmarking protocols. *arXiv preprint arXiv:1502.03143*, 2015. 2, 3, 4, 14

[16] Matthew Chang, Arjun Gupta, and Saurabh Gupta. Semantic visual navigation by watching youtube videos. In *Advances in Neural Information Processing Systems*, 2020. 2

[17] Enric Corona, Albert Pumarola, Guillem Alenya, Francesc Moreno-Noguer, and Grégory Rogez. Ganhand: Predicting human grasp affordances in multi-object scenes. In *Proceedings of the IEEE/CVF Conference on Computer Vision and Pattern Recognition*, pages 5031–5041, 2020. 1, 3

[18] Mehmet R Dogar and Siddhartha S Srinivasa. Push-grasping with dexterous hands: Mechanics and a method. 2010. 2

[19] Yan Duan, Xi Chen, Rein Houthoofd, John Schulman, and Pieter Abbeel. Benchmarking deep reinforcement learning for continuous control. 2016. 2

[20] Justin Fu, Katie Luo, and Sergey Levine. Learning robust rewards with adversarial inverse reinforcement learning. *arXiv*, 2017. 2

- [21] Guillermo Garcia-Hernando, Edward Johns, and Tae-Kyun Kim. Physics-based dexterous manipulations with estimated hand poses and residual reinforcement learning. *arXiv preprint arXiv:2008.03285*, 2020. 3
- [22] Guillermo Garcia-Hernando, Shanxin Yuan, Seungryul Baek, and Tae-Kyun Kim. First-person hand action benchmark with rgb-d videos and 3d hand pose annotations. *CVPR*, pages 409–419, 2018. 3
- [23] Liuhao Ge, Zhou Ren, Yuncheng Li, Zehao Xue, Yingying Wang, Jianfei Cai, and Junsong Yuan. 3d hand shape and pose estimation from a single rgb image. In *CVPR*, pages 10833–10842, 2019. 3
- [24] Shreyas Hampali, Mahdi Rad, Markus Oberweger, and Vincent Lepetit. Honnotate: A method for 3d annotation of hand and object poses. In *CVPR*, 2020. 3
- [25] Ankur Handa, Karl Van Wyk, Wei Yang, Jacky Liang, Yu-Wei Chao, Qian Wan, Stan Birchfield, Nathan Ratliff, and Dieter Fox. Dexpivot: Vision-based teleoperation of dexterous robotic hand-arm system. In *2020 IEEE International Conference on Robotics and Automation (ICRA)*, pages 9164–9170. IEEE, 2020. 5, 6
- [26] Yana Hasson, Gul Varol, Dimitrios Tzionas, Igor Kalevatykh, Michael J Black, Ivan Laptev, and Cordelia Schmid. Learning joint reconstruction of hands and manipulated objects. In *CVPR*, pages 11807–11816, 2019. 1, 3
- [27] Yisheng He, Wei Sun, Haibin Huang, Jianran Liu, Haoqiang Fan, and J. Sun. Pvn3d: A deep point-wise 3d keypoints voting network for 6dof pose estimation. *2020 IEEE/CVF Conference on Computer Vision and Pattern Recognition (CVPR)*, pages 11629–11638, 2020. 3, 4
- [28] Jonathan Ho and Stefano Ermon. Generative adversarial imitation learning. In *NeurIPS*, 2016. 2
- [29] Jonathan Ho and Stefano Ermon. Generative adversarial imitation learning. In *NeurIPS*, pages 4565–4573, 2016. 6
- [30] Yinlin Hu, Joachim Hugonot, Pascal Fua, and Mathieu Salzmann. Segmentation-driven 6d object pose estimation. *CVPR*, pages 3380–3389, 2019. 3
- [31] Umar Iqbal, Pavlo Molchanov, Thomas Breuel Juergen Gall, and Jan Kautz. Hand pose estimation via latent 2.5 d heatmap regression. In *ECCV*, pages 118–134, 2018. 3
- [32] Hanwen Jiang, Shaowei Liu, Jiashun Wang, and Xiaolong Wang. Hand-object contact consistency reasoning for human grasps generation. *arXiv preprint arXiv:2104.03304*, 2021. 3
- [33] Steven G Johnson. The nlopt nonlinear-optimization package, 2014. 6
- [34] Bingyi Kang, Zequn Jie, and Jiashi Feng. Policy optimization with demonstrations. In *International Conference on Machine Learning*, pages 2469–2478. PMLR, 2018. 6
- [35] Hiroharu Kato, Yoshitaka Ushiku, and Tatsuya Harada. Neural 3d mesh renderer. In *Proceedings of the IEEE conference on computer vision and pattern recognition*, pages 3907–3916, 2018. 5
- [36] Wadim Kehl, Fabian Manhardt, Federico Tombari, Slobodan Ilic, and Nassir Navab. Ssd-6d: Making rgb-based 3d detection and 6d pose estimation great again. *ICCV*, pages 1530–1538, 2017. 3
- [37] Shah Mostafa Khaled, Md Saiful Islam, Md Golam Rabbani, Mirza Rehenuma Tabassum, Alim Ul Gias, Md Mostafa Kamal, Hossain Muhammad Muctadir, Asif Khan Shakir, Asif Imran, and Saiful Islam. Combinatorial color space models for skin detection in sub-continental human images. In *International Visual Informatics Conference*, pages 532–542. Springer, 2009. 5
- [38] Dominik Kulon, Riza Alp Guler, Iasonas Kokkinos, Michael M. Bronstein, and Stefanos Zafeiriou. Weakly-supervised mesh-convolutional hand reconstruction in the wild. In *CVPR*, June 2020. 3
- [39] Vikash Kumar, Zhe Xu, and Emanuel Todorov. Fast, strong and compliant pneumatic actuation for dexterous tendon-driven hands. In *2013 IEEE international conference on robotics and automation*, pages 1512–1519. IEEE, 2013. 2, 4, 5
- [40] Shuang Li, Xiaojian Ma, Hongzhuo Liang, Michael Görner, Philipp Ruppel, Bin Fang, Fuchun Sun, and Jianwei Zhang. Vision-based teleoperation of shadow dexterous hand using end-to-end deep neural network. In *2019 International Conference on Robotics and Automation (ICRA)*, pages 416–422. IEEE, 2019. 5
- [41] Fangchen Liu, Zhan Ling, Tongzhou Mu, and Hao Su. State alignment-based imitation learning. In *ICLR*, 2020. 2
- [42] Shaowei Liu, Hanwen Jiang, Jiarui Xu, Sifei Liu, and Xiaolong Wang. Semi-supervised 3d hand-object poses estimation with interactions in time. In *Proceedings of the IEEE conference on computer vision and pattern recognition*, 2021. 3, 5
- [43] YuXuan Liu, Abhishek Gupta, Pieter Abbeel, and Sergey Levine. Imitation from observation: Learning to imitate behaviors from raw video via context translation. In *2018 IEEE International Conference on Robotics and Automation (ICRA)*, pages 1118–1125. IEEE, 2018. 3
- [44] Priyanka Mandikal and Kristen Grauman. Dexterous robotic grasping with object-centric visual affordances. *arXiv preprint arXiv:2009.01439*, 2020. 3
- [45] Andrew Y Ng, Stuart J Russell, et al. Algorithms for inverse reinforcement learning. 2000. 2
- [46] Allison M Okamura, Niels Smaby, and Mark R Cutkosky. An overview of dexterous manipulation. In *Proceedings 2000 ICRA. Millennium Conference. IEEE International Conference on Robotics and Automation. Symposia Proceedings (Cat. No. 00CH37065)*, volume 1, pages 255–262. IEEE, 2000. 2
- [47] OpenAI, Ilge Akkaya, Marcin Andrychowicz, Maciek Chociej, Mateusz Litwin, Bob McGrew, Arthur Petron, Alex Paino, Matthias Plappert, Glenn Powell, Raphael Ribas, Jonas Schneider, Nikolas Tezak, Jerry Tworek, Peter Welinder, Lilian Weng, Qiming Yuan, Wojciech Zaremba, and Lei Zhang. Solving rubik’s cube with a robot hand. *arXiv*, 2019. 1, 2
- [48] OpenAI, Marcin Andrychowicz, Bowen Baker, Maciek Chociej, Rafał Józefowicz, Bob McGrew, Jakub Pachocki, Arthur Petron, Matthias Plappert, Glenn Powell, Alex Ray, Jonas Schneider, Szymon Sidor, Josh Tobin, Peter Welinder, Lilian Weng, and Wojciech Zaremba. Learning dexterous in-hand manipulation. *arXiv*, 2018. 1, 2

- [49] Deepak Pathak, Parsa Mahmoudieh, Guanghao Luo, Pulkit Agrawal, Dian Chen, Yide Shentu, Evan Shelhamer, Jitendra Malik, Alexei A. Efros, and Trevor Darrell. Zero-shot visual imitation. In *ICLR*, 2018. 3
- [50] Sida Peng, Yuan Liu, Qi-Xing Huang, Hujun Bao, and Xiaowei Zhou. Pvnnet: Pixel-wise voting network for 6dof pose estimation. *CVPR*, pages 4556–4565, 2019. 3
- [51] Xue Bin Peng, Erwin Coumans, Tingnan Zhang, Tsang-Wei Lee, Jie Tan, and Sergey Levine. Learning agile robotic locomotion skills by imitating animals. *arXiv preprint arXiv:2004.00784*, 2020. 3
- [52] Xue Bin Peng, Angjoo Kanazawa, Jitendra Malik, Pieter Abbeel, and Sergey Levine. Sfv: Reinforcement learning of physical skills from videos. *TOG*, 2018. 3
- [53] Jan Peters and Stefan Schaal. Reinforcement learning of motor skills with policy gradients. *Neural networks*, 2008. 2
- [54] Dean A Pomerleau. Alvin: An autonomous land vehicle in a neural network. In *NeurIPS*, 1989. 2
- [55] Martin L. Puterman. *Markov Decision Processes: Discrete Stochastic Dynamic Programming*. John Wiley & Sons, Inc., New York, NY, USA, 1st edition, 1994. 6
- [56] Mahdi Rad and Vincent Lepetit. Bb8: A scalable, accurate, robust to partial occlusion method for predicting the 3d poses of challenging objects without using depth. *ICCV*, pages 3848–3856, 2017. 3
- [57] Ilija Radosavovic, Xiaolong Wang, Lerrel Pinto, and Jitendra Malik. State-only imitation learning for dexterous manipulation. *IROS*, 2021. 2, 6, 7
- [58] Aravind Rajeswaran, Vikash Kumar, Abhishek Gupta, Giulia Vezzani, John Schulman, Emanuel Todorov, and Sergey Levine. Learning complex dexterous manipulation with deep reinforcement learning and demonstrations. *arXiv preprint arXiv:1709.10087*, 2017. 6, 7, 14
- [59] Aravind Rajeswaran, Vikash Kumar, Abhishek Gupta, Giulia Vezzani, John Schulman, Emanuel Todorov, and Sergey Levine. Learning complex dexterous manipulation with deep reinforcement learning and demonstrations. 2018. 1, 2, 4
- [60] Robert N Rohling, John M Hollerbach, and Stephen C Jacobsen. Optimized fingertip mapping: a general algorithm for robotic hand teleoperation. *Presence: Teleoperators & Virtual Environments*, 2(3):203–220, 1993. 5, 6
- [61] Javier Romero, Dimitrios Tzionas, and Michael J Black. Embodied hands: Modeling and capturing hands and bodies together. *ToG*, 36(6):245, 2017. 5
- [62] Stéphane Ross and Drew Bagnell. Efficient reductions for imitation learning. In *Proceedings of the thirteenth international conference on artificial intelligence and statistics*, pages 661–668. JMLR Workshop and Conference Proceedings, 2010. 2
- [63] Daniela Rus. In-hand dexterous manipulation of piecewise-smooth 3-d objects. *The International Journal of Robotics Research*, 18(4):355–381, 1999. 2
- [64] Stuart Russell. Learning agents for uncertain environments. 1998. 2
- [65] Karl Schmeckpeper, Oleh Rybkin, Kostas Daniilidis, Sergey Levine, and Chelsea Finn. Reinforcement learning with videos: Combining offline observations with interaction. *arXiv preprint arXiv:2011.06507*, 2020. 1, 2
- [66] Karl Schmeckpeper, Annie Xie, Oleh Rybkin, Stephen Tian, Kostas Daniilidis, Sergey Levine, and Chelsea Finn. Learning predictive models from observation and interaction. *arXiv preprint arXiv:1912.12773*, 2019. 2
- [67] John Schulman, Sergey Levine, Pieter Abbeel, Michael Jordan, and Philipp Moritz. Trust region policy optimization. In *International conference on machine learning*, pages 1889–1897. PMLR, 2015. 7
- [68] Pierre Sermanet, Corey Lynch, Yevgen Chebotar, Jasmine Hsu, Eric Jang, Stefan Schaal, Sergey Levine, and Google Brain. Time-contrastive networks: Self-supervised learning from video. 2018. 3
- [69] Dandan Shan, Jiaqi Geng, Michelle Shu, and David Fouhey. Understanding human hands in contact at internet scale. In *CVPR*, 2020. 5
- [70] Lin Shao, Toki Migimatsu, Qiang Zhang, Karen Yang, and Jeannette Bohg. Concept2robot: Learning manipulation concepts from instructions and human demonstrations. In *Proceedings of Robotics: Science and Systems (RSS)*, 2020. 2
- [71] Pratyusha Sharma, Lekha Mohan, Lerrel Pinto, and Abhinav Gupta. Multiple interactions made easy (mime): Large scale demonstrations data for imitation. *arXiv*, 2018. 3
- [72] Pratyusha Sharma, Deepak Pathak, and Abhinav Gupta. Third-person visual imitation learning via decoupled hierarchical controller. In *NeurIPS*, 2019. 3
- [73] Maximilian Sieb, Zhou Xian, Audrey Huang, Oliver Kroemer, and Katerina Fragkiadaki. Graph-structured visual imitation. In *Conference on Robot Learning*, pages 979–989. PMLR, 2020. 3
- [74] Laura Smith, Nikita Dhawan, Marvin Zhang, Pieter Abbeel, and Sergey Levine. Avid: Learning multi-stage tasks via pixel-level translation of human videos. *arXiv preprint arXiv:1912.04443*, 2019. 3
- [75] Shuran Song, Andy Zeng, Johnny Lee, and Thomas Funkhouser. Grasping in the wild: Learning 6dof closed-loop grasping from low-cost demonstrations. *Robotics and Automation Letters*, 2020. 2
- [76] Adrian Spurr, Jie Song, Seonwook Park, and Otmar Hilliges. Cross-modal deep variational hand pose estimation. In *CVPR*, 2018. 3
- [77] Richard S Sutton and Andrew G Barto. *Introduction to Reinforcement Learning*, volume 135. MIT press, 1998. 6
- [78] Omid Taheri, Nima Ghorbani, Michael J Black, and Dimitrios Tzionas. Grab: A dataset of whole-body human grasping of objects. In *European Conference on Computer Vision*, pages 581–600. Springer, 2020. 3
- [79] Bugra Tekin, Sudipta N. Sinha, and Pascal Fua. Real-time seamless single shot 6d object pose prediction. *CVPR*, pages 292–301, 2018. 3
- [80] Emanuel Todorov, Tom Erez, and Yuval Tassa. Mujoco: A physics engine for model-based control. In *2012 IEEE/RSJ International Conference on Intelligent Robots and Systems*, pages 5026–5033. IEEE, 2012. 4, 14
- [81] Emanuel Todorov and Michael I Jordan. Smoothness maximization along a predefined path accurately predicts the speed profiles of complex arm movements. *Journal of Neurophysiology*, 80(2):696–714, 1998. 6

- [82] Faraz Torabi, Garrett Warnell, and Peter Stone. Behavioral cloning from observation. *arXiv*, 2018. 2
- [83] Faraz Torabi, Garrett Warnell, and Peter Stone. Generative adversarial imitation from observation. *arXiv*, 2018. 2
- [84] Matej Večerík, Todd Hester, Jonathan Scholz, Fumin Wang, Olivier Pietquin, Bilal Piot, Nicolas Heess, Thomas Rothörl, Thomas Lampe, and Martin Riedmiller. Leveraging demonstrations for deep reinforcement learning on robotics problems with sparse rewards. *arXiv*, 2017. 2
- [85] Yu Xiang, Tanner Schmidt, Venkatraman Narayanan, and Dieter Fox. Posecnn: A convolutional neural network for 6d object pose estimation in cluttered scenes. *ArXiv*, abs/1711.00199, 2018. 1, 3
- [86] Sarah Young, Dhiraj Gandhi, Shubham Tulsiani, Abhinav Gupta, Pieter Abbeel, and Lerrel Pinto. Visual imitation made easy. *arXiv e-prints*, pages arXiv–2008, 2020. 2
- [87] Christian Zimmermann and Thomas Brox. Learning to estimate 3d hand pose from single rgb images. In *CVPR*, pages 4903–4911, 2017. 3
- [88] Christian Zimmermann, Duygu Ceylan, Jimei Yang, Bryan Russell, Max Argus, and Thomas Brox. Freihand: A dataset for markerless capture of hand pose and shape from single rgb images. In *Proceedings of the IEEE/CVF International Conference on Computer Vision*, pages 813–822, 2019. 3

Appendices

A. Overview

This supplementary material provides more details, results and visualizations accompanying the main paper. In summary, we include

- More details about video data collection;
- More details about the *Relocate*, *Pour*, and *Place inside* environments;
- More details about hand motion retargeting and demonstration generation in DexMV pipeline;
- More visualization of hand-object pose estimation and hand motion retargeting results.

B. Video Data Collection

We use Intel RealSense D435 cameras to collect human demonstrations of manipulating different objects for finishing diverse tasks on table. In detail, each captured demonstration is about 10 seconds. Moreover, after the demonstration is captured, only the pour task is in need to reset the particles back into the mug, which tasks about 6 seconds. Thus, the time cost for data collection is not high, and the procedure tends to be scalable on different objects and tasks. In practice, it takes about 60 minutes to capture all 100 sequences for a task.

C. Environments

We propose three types of manipulation tasks along with the DexMV Platform: *Relocate*, *Pour*, and *Place Inside*. The manipulated objects come from YCB Dataset [15]. Environments use the MuJoCo simulator [80] with timestep set to 0.002 and frame skip set to 5. We adopt the same contact friction parameters following the setting in the literature [58]. We use the open-source MuJoCo model of Adroit Hand provided here¹. Figure 11 shows the seven different task used in DexMV: *Relocate* with five different objects, *Pour*, and *Place Inside*.

Action: the action space is the same for all tasks, which is the motor command of 30 actuators on the robotic hand. The first 6 motors control the global position and orientation of the robot while the last 24 motors control the fingers of the hand. We normalize the action range to $(-1, 1)$ based on actuator specification.

¹<https://github.com/vikashplus/Adroit>

C.1. Relocate

Observation: the observation of *Relocate* is composed of four components: (i) joint angles of adroit hands; (ii) global position of adroit hands root; (iii) object position; (iv) target position. The overall observation space is 39-dim.

Reward: the reward is defined based on three distances: (i) the distance between the robot hand and the object; (ii) the distance between the robot hand and the target; (iii) the distance between the object and the target. The lower the distance is, the higher the reward is.

Reset: for each episode, the xy position of both object and target is randomized within a $(-0.3, 0.3)$ square on the table. The height of target is randomized between $(0.15, 0.25)$.

C.2. Pour

Observation: Similar to *Relocate*, we use the robot joint angles, root position of robot hand, and object position, in the observation. In *Pour*, we replace the target position with container position. In addition, since the agent needs orientation information of the mug to pour the water particles, we add quaternion to represent object orientation.

Reward: The main reward is based on the final number of particles that fell within container. Additionally, similar to *Relocate*, we use the distance between the robot hand and the object as well as the distance between the object and the container to provide part of the rewards. The lower the distance is, the higher the reward is. The coefficient of the main reward is $10\times$ larger than the reward computed based on the distance.

Reset: For each episode, the xy position of the mug is randomized between $(-0.1, 0.1)$ on the table. The water particles are inside the mug at the beginning of each episode. The container is always at the center of the table top.

C.3. Place Inside

Observation: The observation space of the *Place Inside* task is exactly the same as the observation space of *Pour* as described in Section C.2.

Reward: The main reward is based on the position and orientation of the manipulated object. If the object is placed inside of the mug, the agent will get a large portion of reward. Similar to *Relocate*, we also add a lifting reward to encourage the robot to first lift the object up before moving it towards the container.

Reset: For each episode, the xy position of the object is randomized between $(-0.15, 0.15)$ on the table. The container, i.e. mug, is always placed at the center of table top.

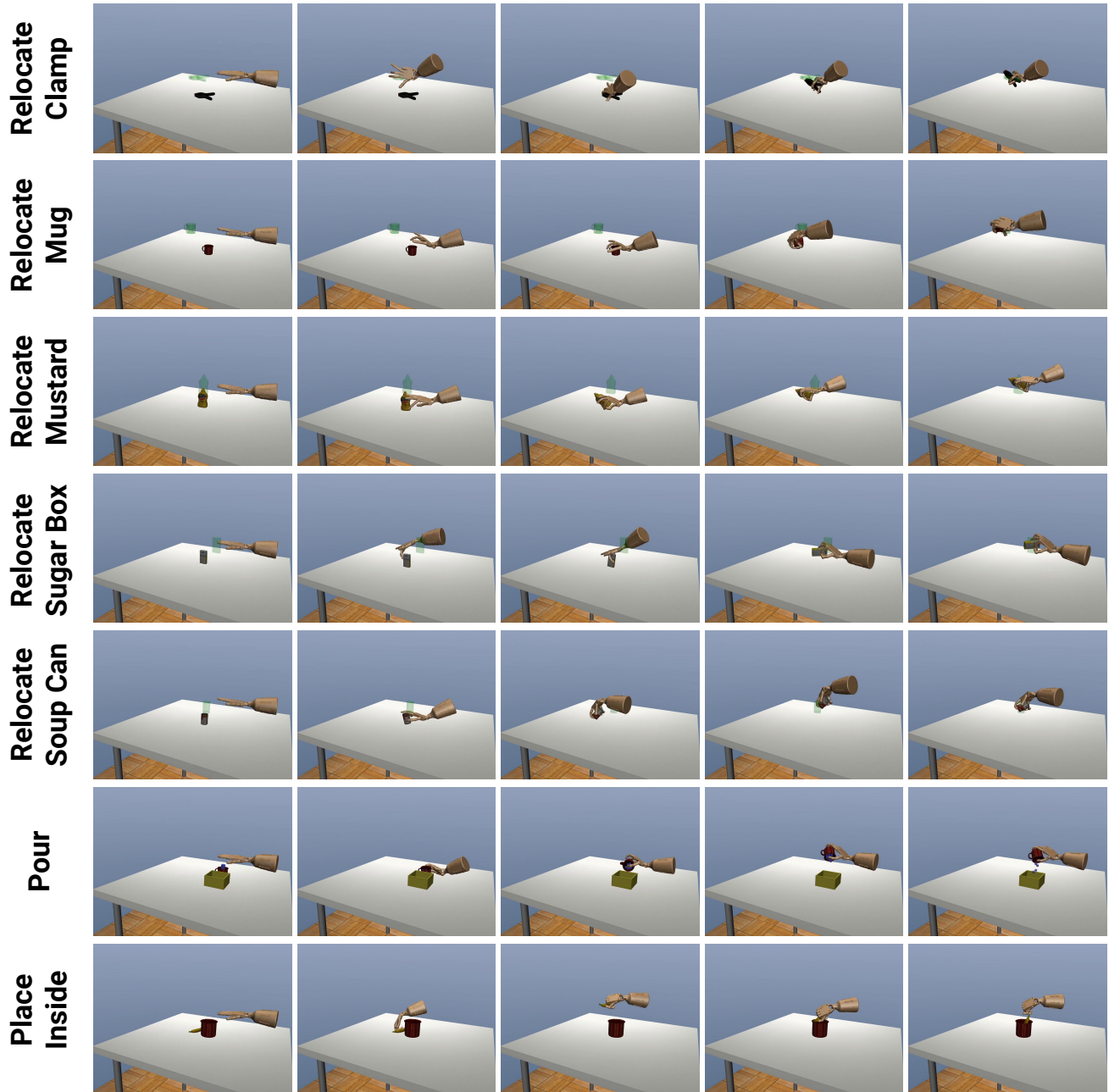


Figure 11: **DexMV Tasks.** There are three types of tasks in the figure. The first five columns: *relocate* with mug, mustard bottle, clamp, sugar box, tomato soup can. *Relocate* task means that the agent needs to move the object from the initial position to the target position. The sixth and seventh columns: *Pour* and *Place Inside*. In *Pour* task, the agent needs to pour the water particles inside a mug into the yellow container. In *Place Inside* task, the agent needs to manipulate the orientation of the banana to place it inside a mug. Both of the last two tasks require delicate manipulation.

D. Demonstration Generation

D.1. Kinematics Model

In Table 3, we compare the difference of kinematics model between human hand and robot hand. The overall Degree-of-Freedom(DoF) of human hand is higher than the

DoF of robot hand. Thus hand motion retargeting from human to robot is projecting a pose from a higher dimension to a lower dimension, which will lose information inevitably. The motion retargeting module try to maintain the fingertip positions, which often contact points between hand and object, between these two different kinematics model.

	H-Joints	H-DoF	R-Joints	R-DoF
Thumb	3x Ball	9	5x Revolute	5
Index	3x Ball	9	4x Revolute	4
Middle	3x Ball	9	4x Revolute	4
Ring	3x Ball	9	4x Revolute	4
Pinkie	3x Ball	9	5x Revolute	5
Wrist	Null	0	2x Revolute	2
Root	1x Free	6	1x Free	6
Overall	N/A	51	N/A	30

Table 3: **Comparison of Kinematics** We compare the kinematic model between MANO human hand and the robot hand we used in simulator. **H** is the abbr for Human while **R** stands for robot. For example, the **H-Joints** column shows the number and type of joints for a specific sub-part in the kinematics model. Each ball joint has 3 Degree-of-Freedom(DoF), each revolute joint has 1 DoF, and each free joint has 6 DoF

D.2. Hand Motion Retargeting

As mentioned in the main paper, to compute the pose of robot hand, we minimize the difference of ten task space vectors between human and robot hand. The ten task space vectors include the vector from wrist to proximal phalanx and the vector from proximal phalanx to tip for each finger. The objective function of the optimization problem is shown as follow:

$$\min_q \sum_{i=0}^N \|v_i^H - v_i^R(q)\|^2 + \alpha \|q - q_{last}\|^2 \quad (4)$$

, where q is a 30-d vector represents the robot joint angles and q_{last} is the optimized joint angle from the last optimization step or a zero vector for the first pose in the sequence. v_i^H is the i -th task space vector for human hand while the v_i^R is the i -th task space vector for robot hand. Besides, we find that adding the normalization term can improve the temporal consistency and avoid a bad local minimum. Also, we use the q_{last} as the initial value during the optimization. We use $N = 10$ and $\alpha = 8e - 3$ in our implementation.

D.3. Imitation Data Generation

Filter Estimated Pose: When human is manipulating the object, either hand or object is in heavy occlusion, which may cause inconsistent estimation results. To improve the temporal consistency of the estimated hand and object poses, we apply a second-order digital low-pass filter to remove the high frequency noise. The sampling frequency of the filter is 100 while the cutoff frequency is 5 for the position of both object and hand. Filtering the rotation is not as straightforward as filtering the position. To get smooth orientation sequence, we first convert the rotation into $so(3)$ lie algebra. Then, we apply the filter in $so(3)$ space and

convert it back to rotation matrix $SO(3)$ after filtering.

Align Time Step: Another issue is the time step. The action frequency of the RL agent is 100Hz, which is higher than the video capture frequency of 25Hz. However, when training an imitation learning algorithm, the demonstration needs to follow the specification of the environment, which needs to be 100Hz. To align the time step between estimated hand and object pose to 100Hz, the position is interpolated using a cubic spline function. For the orientation part, we first compute the relative rotation between two consecutive frames. Similar as rotation filtering, the relative rotation is converted to $so(3)$ and be interpolated in that space and then converted back to rotation matrix.

Select Target Position: In *Relocate* task, the goal-conditioned agent needs to move the object to a target position, which is randomized for each episode as mentioned in Section C. The target position information is also included in the observation space of the agent. In the demonstration, we use the position of the object in the last frame after filtering as the target position.

E. More Visualization of Hand-Object Pose Estimation and Hand Motion Retargeting

In this section, we provide more visualization on hand-object pose estimation and hand motion retargeting in Figure 12. The four tasks in the first three rows are: *Relocate* with tomato soup can, sugar box, mustard bottle, and mug. The three tasks in the last three rows are: *Relocate* with clamp, *Pour*, and *Place Inside*.

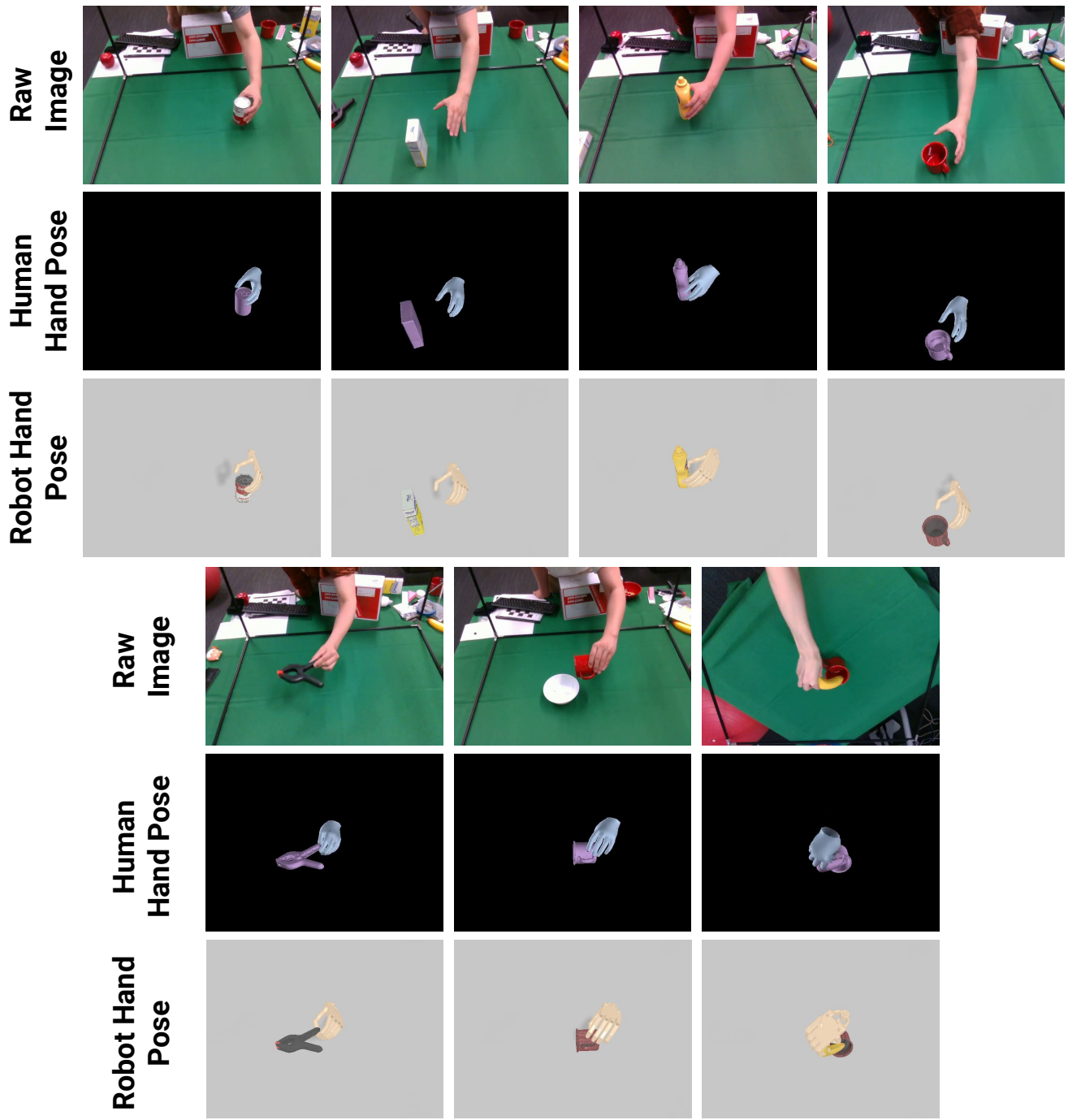


Figure 12: **3D hand-object pose estimation results and hand motion retargeting results.** Visualization on relocate tomato soup can, sugar box, mustard bottle, mug, clamp, pour, and place inside.